Towards population-based structural health monitoring, Part I: Homogeneous populations and forms

L.A. Bull[1], P.A. Gardner[1], J. Gosliga[1], N. Dervilis[1], E. Papatheou[2], A.E. Maguire[3], C. Campos[3], T.J. Rogers[1], E.J. Cross[1], & K. Worden[1]

[1]Dynamics Research Group, Department of Mechanical Engineering
University of Sheffield, Mappin Street, Sheffield S1 3JD, UK
[2]College of Engineering Mathematics and Physical Sciences
University of Exeter, Exeter EX4 4QF, UK
[3]Vattenfall Research and Development, New Renewables,
The Tun Building, Holyrood Road, Edinburgh EH8 8AE, UK

Abstract

Data-driven models in Structural Health Monitoring (SHM) generally require comprehensive datasets, recorded from systems in operation, which are rarely available. One potential solution to this problem, considers that information might be transferred, in some sense, between *similar* systems. As a result, a *population-based* approach to SHM suggests methods to *both* model and transfer this valuable information, by considering different groups of structures as populations. Specifically, in this work, a method is proposed to model a population of *nominally-identical* systems, where (complete) datasets are only available from a subset of members. The framework attempts to build a general model, referred to as the population *form*, which can be used to make predictions across a group of homogeneous systems. First, the form is demonstrated through applications to a simulated population – with a single experimental (test-rig) member; secondly, the form is applied to data recorded from a group of operational wind turbines.

Keywords: Population-based Structural Health Monitoring; Homogeneous Populations

1 Population-based SHM

Conventionally in Structural Health Monitoring (SHM), a predictive model is learnt using the data recorded from a single system, and the model is expected to generalise to future measurements from that system in operation. For a given structure, however, the recorded signals are usually limited; corresponding to only a fraction of the potential operational, environmental and damaged conditions; additionally, the label set (used to describe what each of the measured signals represents) might be unavailable or incomplete. In consequence, if a framework can transfer this missing information between groups of *similar* structures, it should bring significant advantages to practical applications of SHM.

This issue of missing information motivates a *population-based* approach to SHM [1, 2, 3, 4, 5, 6, 7]. The aim of this new technology is to facilitate the transfer of valuable knowledge between groups of *similar* systems, i.e. *populations*. Intuitively, the *type* of population is important, as this will define *what knowledge* can be transferred, and by *what method*. This paper focusses on the most obvious (and conceptually basic) type of population, in which all members within the group can be (informally) considered as *nominally-identical* [3]; for example, wind turbines within a wind farm. Such a population is refereed to as *homogeneous*, and in certain cases, a general model (referred to here as the population *form*) can used to represent the behaviour of the entire population, and infer the presence of damage across the group.

Importantly, this paper is the first in a series [2, 5, 6, 7] introducing various methods for population-based SHM. While this work focusses on the most uniform case – the application of a population *form* to model nominally-identical

systems – papers [2, 4, 5] concern more involved technologies, of a different nature. These methods are introduced by considering (and defining) groups of structures beyond the nominally-identical case; more specifically, *heterogeneous* populations. These populations can contain more disparate members - for example, different designs of suspension bridge. While these structures may still be similar, they are clearly not nominally identical.

The layout of this paper is as follows. Section 2 attempts to (more rigorously) define homogeneous populations, including the *strongly*-homogeneous case; the *form* is also defined, which can be applied in certain realisations. Section 3 extends a simulated case study (introduced in [3]), to demonstrate the form for the *strongly*-homogeneous case. Through applications to measured data from an operational wind farm, Section 4 demonstrates how the complexity of the from can be increased, to model the population behaviour, even when it no longer represents the strongly-homogeneous case. Finally, Section 5 discusses the limitations of the form (*applied in this work*) and suggests alternative methods (and forms) that could be used represent homogeneous populations as thier behaviour becomes more complex.

2 Homogeneous populations and forms

A convenient language to define homogeneous (as well as heterogeneous) populations borrows terminology from graph theory; these ideas are formally introduced in the context of structures in papers [2, 4] of the series. For clarity, definitions are provided with general terminology here, however, these relate directly to the ideas presented in [2, 4].

An important relation is *structural equivalence*; briefly, this implies that the graphs used to represent structures are *topologically equivalent*, with ground-nodes occurring in the same location – an example of two structurally-equivalent graphs is presented in Figure 1.

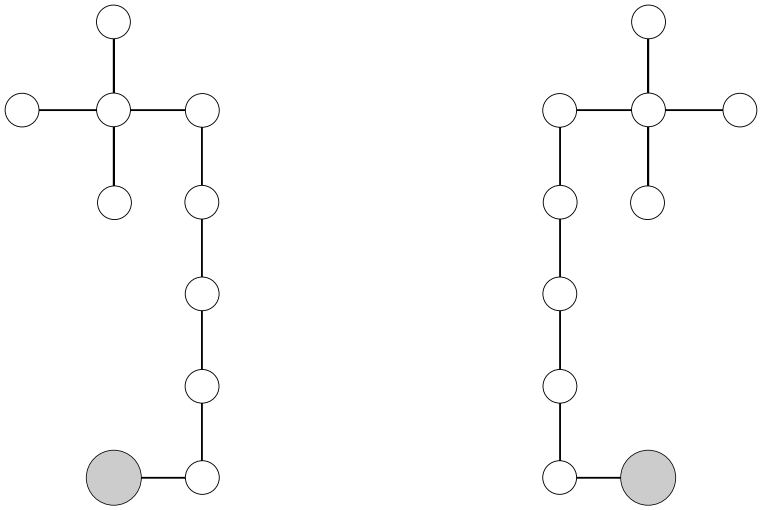

Figure 1: Two (trivially) *topologically-equivalent* graphs, that could be used to represent to *stucturally-equivalent* wind trubines. Ground nodes are shaded.

This then leads to:

Definition 1. *A population of M structures $\{S_i\}_{i=1}^{M}$ is homogeneous if the individual members are pair-wise structurally equivalent, with material, geometric, and physical parameters $\boldsymbol{\Theta}_i$ (i.e. graph attributes) that can be considered as random draws from an underlying base-distribution $p(\boldsymbol{\Theta}_i)$.*

As a result, the distribution $p(\boldsymbol{\Theta}_i)$ captures the population variance. If any pair of members are not structurally equivalent, the population is *heterogeneous*.

2.1 Strongly-homogeneous populations

A further restriction considers the *strongly*-homogeneous case. In this scenario, the densities $p(\boldsymbol{\Theta}_i)$ associated with the parameters of the population (attributes from the associated graphs [2]) are considered to be 'compact' and unimodal. In the strictest sense, the associated densities would be Dirac functions over the parameter values, such that each member is an identical system. A more realistic example, however, considers a population of structures which are all the same model but subject to manufacturing tolerances. Generally, in this setting, methods from conventional SHM [8] can be applied to population data, as demonstrated in the first case study, in Section 3 here.

It is important to note, however, that a strongly-homogeneous population represents an ideal-case. Returning to the wind farm example, while the population is homogeneous in terms of structural equivalence, it is unlikely that the structures will be *strongly*-homogeneous. For example, consider the complex distributions that will (inevitably) be associated with the parameters relating to the boundary conditions at the seabed, or local interactions with the wind, as well as differences relating to operational practice. In consequence, the second case study (Section 4) demonstrates one method for moving beyond the strongly homogeneous case.

2.2 The population form

In general terms, the form is *some* model that can be used to represent a population of homogeneous systems; therefore, it can be considered as a generic representation of the population; more specifically [3],

Definition 2. *The population form is any combination of model and/or feature space that can be used as a representation of a population of systems, in the context of SHM.*

In view of this definition, the model should be validated within the population and chosen feature space, such that it is capable of representing the variation between individuals. While variation between members is not significant when applying the form to the strongly-homogeneous case, upon moving to more realistic examples, the form must become more complex to capture variation between members – as will be demonstrated in the case studies. As a result, a more diverse set of alternative technologies become relevant.

In the case studies here, a functional (statistical) model of the form (Gaussian process regression [9]) is defined using the available benchmark normal-condition data. Importantly, these data are incomplete (or absent) from several members within the population. Through comparisons between future measurements and the form, the model can be used to inform novelty detection across the entire population, in order to monitor the condition of each member.

2.2.1 Gaussian process regression as a functional representation of the form

As discussed, any suitable combination of model and/or feature space can be used to represent the population form. In this work, as *functional features* are used in both case studies, a regression tool is applied – specifically, Gaussian Process (GP) regression[1]. Gaussian processes can be used to solve regression problems through a Bayesian machine learning approach [9, 10]. The GPs exhibit a number of desirable properties for this application: they are non-parametric, automatically return confidence intervals, and they are capable of modelling data with a low signal-to-noise ratio. A brief review of the theory is provided here; details can be found in [9, 10].

For a set of N inputs $\mathbf{x}_i$, and corresponding outputs y_i, (i.e. training data, $\mathcal{D} = \{\mathbf{x}_i, y_i\}_{i=1}^{N}$) GP regression looks to define the predictive distribution, given a new input $\mathbf{x}_*$ and the available training data $\mathcal{D}$. Specifically, it is assumed that the observations can be modelled by some noiseless latent function f of the inputs, plus an independent noise term, ϵ [11],

$$y = f(\mathbf{x}) + \epsilon \tag{1}$$

A zero-mean GP prior is set over the latent functions f, with covariance function $k(\mathbf{x}, \mathbf{x}')$, and a Gaussian prior is placed over the noise term, such that,

$$f(\mathbf{x}) \sim \mathcal{GP}\left(\mathbf{0}, k(\mathbf{x}, \mathbf{x}')\right), \qquad \epsilon \sim \mathcal{N}(0, \sigma^2) \tag{2}$$

[1] In each case study, a more specific (i.e. parametric) regression model could arguably be applied; however, the focus of this work is to introduce the concept of the *form* for population-based SHM; therefore, GPs are used here as a *general* regression tool, to represent functional forms.

This expression introduces the first hyperparameter σ^2, which specifies the noise variance. To justify the zero-mean assumption, the data are usually normalised by subtracting the sample mean and dividing by the standard deviation [9].

The covariance function encodes the degree of coupling between $y(\mathbf{x})$ and $y(\mathbf{x}')$, and therefore determines the properties of the GP, including the process variance, and smoothness, etc [11]. One of the best-known covariance functions is the squared-exponential, and it is applied in this work,

$$k(\mathbf{x}, \mathbf{x}') = \sigma_0^2 \exp\left(-\frac{1}{2l^2}(\mathbf{x} - \mathbf{x}')\right) \tag{3}$$

This equation defines two more hyperparameters: the length-scale l, and the process variance σ_0. The length scale determines how fast the correlation between outputs decays across the input space, while the process variance determines the power of the signal [11]. Collectively, hyperparameters of the model are $\theta = \{l, \sigma_0, \sigma\}$.

The joint distribution between the training data $\mathcal{D} = \{\mathbf{x}_i, y_i\}_{i=1}^N$ and some unseen observation $\{\mathbf{x}_*, y_*\}$ is a multivariate Gaussian,

$$\begin{bmatrix} \mathbf{y} \\ y_* \end{bmatrix} \sim \mathcal{N}\left(\begin{bmatrix} \mathbf{0} \\ \mathbf{0} \end{bmatrix}, \begin{bmatrix} K_{\mathbf{xx}} + \sigma^2 \mathbf{I}_N & \mathbf{k}_{\mathbf{x},\mathbf{x}_*} \\ \mathbf{k}_{\mathbf{x}_*,\mathbf{x}} & k(\mathbf{x}_*\mathbf{x}_*) + \sigma^2 \end{bmatrix}\right). \tag{4}$$

where $[K_{\mathbf{xx}}]_{ii'} = k(\mathbf{x}_i, \mathbf{x}_{i'})$, $[\mathbf{k}_{\mathbf{x}_i,\mathbf{x}_*}]_i = k(\mathbf{x}_i, \mathbf{x}_*)$, and $[\mathbf{k}_{\mathbf{x}_*,\mathbf{x}_i}]_i = k(\mathbf{x}_*, \mathbf{x}_i)$. $\mathbf{I}_N$ is an $N \times N$ identity matrix. The notation $[A]_{ii'}$ refers to the i^{th} row in column i' of matrix A, while $[\mathbf{a}]_i$ is the i^{th} element of vector $\mathbf{a}$ [11].

By conditioning the joint distribution in (4) on the observed training data in $\mathcal{D}$, the predictive distributions over y_* can be defined [9],

$$\begin{aligned} &p(y_* \mid \mathbf{x}_*, \mathcal{D}) = \mathcal{N}(\mathbb{E}[y_*], \mathbb{V}[y_*]), \\ &\mathbb{E}[y^*] = \mathbf{k}_{\mathbf{x}^*\mathbf{x}} \left(K_{\mathbf{xx}} + \sigma^2 \mathbf{I}_N\right)^{-1} \mathbf{y}, \\ &\mathbb{V}[y^*] = k(\mathbf{x}^*, \mathbf{x}^*) - \mathbf{k}_{\mathbf{x}^*\mathbf{x}} \left(K_{\mathbf{xx}} + \sigma^2 \mathbf{I}_N\right)^{-1} \mathbf{k}_{\mathbf{xx}^*} + \sigma^2 \end{aligned} \tag{5}$$

In order to learn the hyperparameters, $\theta = \{l, \sigma, \sigma_0\}$, a Type-II maximum likelihood approach is taken [9]; this is equivalent to empirical Bayes [12]. As such, the *marginal likelihood* of the model is maximised, $p(y \mid \mathbf{x}, \theta)$; this utilises the Bayesian Occam's razor [13, 9], to find the minimally-complex model given the observed training data $\mathcal{D}$. This optimisation is normally performed as a minimisation over the negative log-marginal-likelihood, for convenience and numerical stability. Therefore, the hyperparameters are estimated through the following optimisation [12],

$$\hat{\theta} = \underset{\theta}{\operatorname{argmin}} \left\{ -\log\, p(y \mid \mathbf{x},\, \theta) \right\}, \tag{6}$$

where,

$$\begin{aligned} -\log\, p(y \mid \mathbf{x},\, \theta) &= -\log\, \mathcal{N}\left(\mathbf{y} \mid \mathbf{0}, K_{\mathbf{x},\mathbf{x}} + \sigma^2 \mathbf{I}_N\right) \\ &= \frac{N}{2} \log\left(2\pi\right) + \frac{1}{2} \log\left|K_{\mathbf{x},\mathbf{x}} + \sigma^2 \mathbf{I}_N\right| + \frac{1}{2}\left[\mathbf{y}^\top \left(K_{\mathbf{xx}} + \sigma^2 \mathbf{I}_N\right)^{-1} \mathbf{y}\right] \end{aligned} \tag{7}$$

3 Case study I: Strongly-homogeneous populations

To demonstrate the form applied to a *strongly homogeneous* population, 19 structurally-equivalent structures are simulated, leading to $\{S_i\}_{i=1}^{19}$. As in previous work [3], each member S_i is defined as a realisation of an experimental rig, designed at the Los Alamos National laboratory [8]; the test-rig acts as the 20^{th} member in the population, such

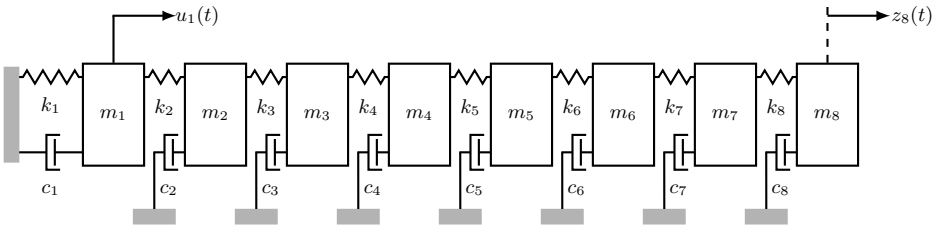

Figure 2: The 8-DOF system

that the total group is $\{S_i\}_{i=1}^{20}$. A schematic of the 8-DOF system is shown in Figure 2; $u_i(t)$ is the system input (forcing) on mass i at time t, and $y_i(t)$ is the system response (output) of mass i at time t.

The system parameters – mass m, stiffness k and damping c – are identified by minimising a sum-of-squares error between the simulated and experimental frequency response functions (FRFs). Briefly, this approach involves simulating the 8DOF test-rig by representing the system equations in state variable form [14, 15]. Following some initial guesses, m, k and c are iteratively updated, while minimising the sum-of-squares error between the simulated FRF and the measured FRFs. A constrained optimisation, based on prior knowledge of the experimental rig, leads to the parameter estimates presented in Table 1. The j index indicates the j^{th} degree of freedom. The first spring stiffness is set to near zero, to correspond to the rigid-body mode of the rig. The forcing, $u_1(t)$, is applied to mass 1, while the response, denoted $\mathbf{z}(t)$, is simulated for all masses and monitored at mass 8, $z_8(t)$.

Table 1: **System parameters**

j	1	2	3	4	5	6	7	8
m_j (kg)	0.5707	0.4202	0.4119	0.4197	0.4197	0.4201	0.4200	0.4199
k_j (kN/M)	0.000	64.810	58.104	56.474	59.556	65.969	65.275	60.121
c_j (Ns/m)	5.43	13.66	11.56	11.71	11.86	13.2	5.55	0.13

3.1 Simulating strongly-homogeneous members

For this simple 8-DOF example, the parameters $\mathbf{\Theta}_i$ (that would be associated with each member in the population S_i) can be considered to be,

$$\mathbf{\Theta}_i = \left\{ m_j^{(i)}, k_j^{(i)}, c_j^{(i)} \right\}_{j=1}^{8} \tag{8}$$

In order to build a *strongly* homogeneous-population, as defined in Section 2.1, the densities $p(\mathbf{\Theta}_i)$ that describe the underlying distribution of these parameters (across the population) should be 'compact' and unimodal; thus, Gaussian distributions are placed over each of the parameter estimates from Table 1, such that,

$$\begin{aligned} m_j^{(i)} &\sim \mathcal{N}(m_j,\, 0.03 \times m_j) \\ k_j^{(i)} &\sim \mathcal{N}(k_j,\, 0.01 \times k_j) \\ c_j^{(i)} &\sim \mathcal{N}(c_j,\, 0.20 \times c_j) \end{aligned} \tag{9}$$

According to Section 2.1, a strongly-homogeneous population can now be generated by randomly drawing parameter sets $\mathbf{\Theta}_i$ from these distributions, to define 19 members.

3.1.1 The Frequency Response Function (FRF) for damage detection

In the context of dynamics-based monitoring, it is generally expected that damage will manifest itself as alterations in the structural parameters – specifically, a reduction in stiffness [8, 16]. Changes in the structural stiffness will alter the dynamic characteristics, therefore, frequency domain observations can be used to (indirectly) monitor any physical

changes that could relate to damage (although such features will also be sensitive to confounding influences [8]. Therefore, the frequency response function (FRF) (denoted by $H(\omega)$) is selected as a frequency-domain observation; this also matches the experimental data recorded at LANL. Specifically, the FRF here is the ratio of the output acceleration at mass eight $\ddot{z}_8(t)$, to the spectrum of the input forcing time series at mass one $u_1(t)$. As with the experimental data, the input is a white-noise excitation over 8s, with a sample-rate of 400.25Hz. A Hanning window is applied to the 8s input and output time series, and the empirical FRF is calculated. The resulting FRF is truncated, such that there are 1040 bins in the frequency domain, ranging from 0 - 130 Hz. Measurement noise is added to the outputs to represent the experimental measurements recorded at LANL; the noise assumed to be zero-mean normally-distributed, with variance leading to a signal-to-noise ratio of 40dB.

Each FRF is considered to be an observation of the system in terms of the SHM strategy, and these observations are used to inform damage detection. Following the same procedure as the practical experiments [8], the stiffness of k_5 is reduced to imitate damage. Reductions are 7%, 14% and 24% for the simulated members, and a single reduction of 24% for data recorded from the test rig.

The FRF is widely used as a functional feature in the conventional SHM literature [8]; as discussed, such methods should apply to the population-based approach, in the restricted strongly-homogeneous case.

3.1.2 Dataset summary

The dataset represents a population of *twenty* 8-DOF systems, 19 are simulated, while the 20^{th} member is the LANL test-rig. Each system is observed over time, through the FRFs estimated from 8s time-windows. Each FRF in the dataset has 1040 frequency bins.

Measurements from the simulated members are defined such that:

- For the normal-condition data, there are 20 FRFs from each stucture. These data are shown by black markers in Figure 3.
- 20 additional normal-condition FRFs are simulated to validate the form. These data are shown by magenta markers in Figure 3.
- 20 FRFs are generated for each of the three states of damage (7%, 14% and 24%), shown by red markers in Figure 3.

The experimental data, recorded from the test-rig, includes:

- 8 FRFs — four correspond to the undamaged state, and four were recorded following the introduction of damage (24% only). In Figure 3, the normal and damaged test-data are also shown by magenta and red markers respectively.

It should be observed from Figure 3 that, while the normal-condition FRFs are similar, population variation can still be observed within the associated FRFs.

3.2 Gaussian Process regression of the FRF as the population form

Considering Section 2.2.1, the GP prior is set as zero-mean; therefore, the real and imaginary parts of the FRF (H) are regressed independently, with two distinct GPs, such that,

$$f(x) + \epsilon = \mathrm{Re}\big[H(\omega)\big] \,, \quad x \triangleq \omega \tag{10}$$

or,

$$f(x) + \epsilon = \mathrm{Im}\big[H(\omega)\big] \,, \quad x \triangleq \omega \tag{11}$$

This approach is adopted – rather than regressing the phases and magnitudes – as it is better suited to the proposed, *general* formulation of the GP. Modelling the FRF with two regressors fails to capture covariance between the outputs; in fact, for a linear system, one function completely determines the other [17]; thus, it is only really necessary to model one output.

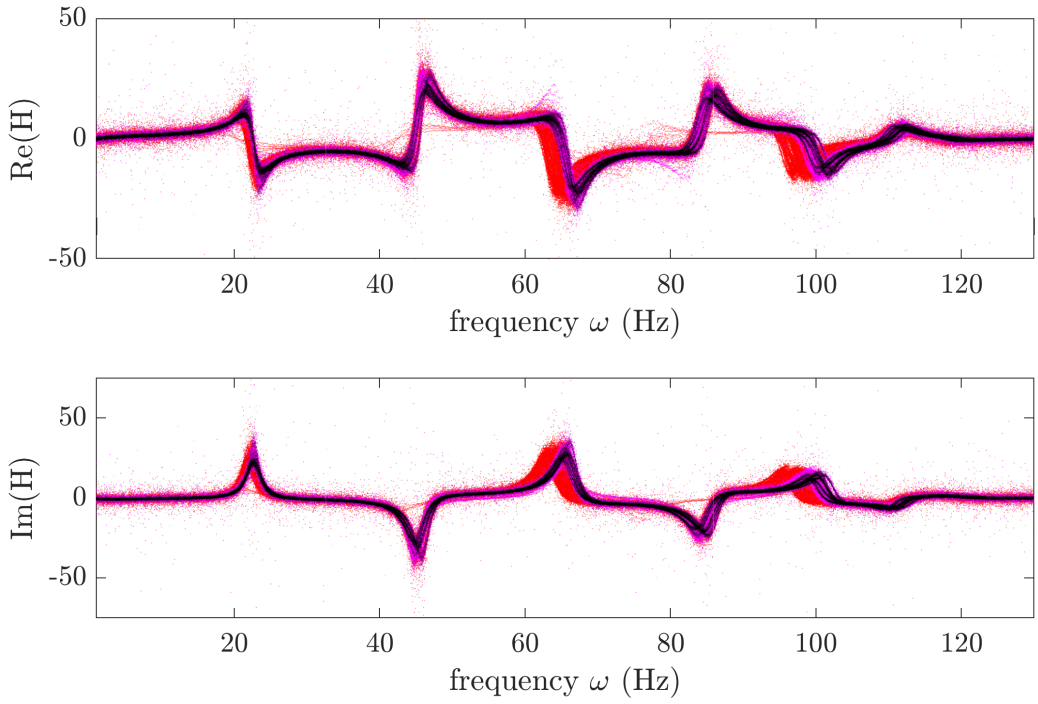

Figure 3: FRF data across a population of twenty 8DOF systems, 19 members are simulated and the 20^{th} member is the experimental rig. For the simulated and experimental systems, normal-condition data are shown by black markers and magenta markers, while the damaged data are shown by red markers.

Importantly, only systems $\{S_1, \ldots, S_{10}\}$ within the population contribute training data to learn the form. The remaining 10 systems $\{S_{11}, \ldots, S_{20}\}$ (nine simulated systems and the experimental rig) are *held-out* of the training process. This choice is made to test the generalisation of the form, when applied to *new* members within the strongly-homogeneous case.

To reduce the computational load, the GP regression is trained using a random sub-sample of 5000 inputs and outputs from the simulated normal-condition data. A more rigorous approach for dealing with large datasets, such as sparse GPs [18], is being considered for future work. The resulting GP representation of the form, and the data used to train it, are illustrated in Figure 4.

3.2.1 Novelty detection via the form

The form can now be used to monitor future data and inform damage detection. In this example, test FRF data from *all* the members in the population are compared to the form; however, to reiterate, of the twenty members, only $\{S_1, \ldots, S_{10}\}$ contributed to training-set. The MSD is useful in this application, as it considers both the mean and the variance of the regression. Therefore, the averaged, univariate MSD is defined for the 1000-point random-sample from each FRF in the test-set, 500 samples from both the real and imaginary parts,

$$MSD_i = \frac{1}{\mathbb{V}[y^*]}(\mathbb{E}[y^*] - \tilde{y}_i)^2 \tag{12}$$

$$MSD_{FRF} = \frac{1}{1000}\sum_{i=1}^{1000} MSD_i \tag{13}$$

The expected values are defined by the predictive equations of the GP in (5), and the tilde is used to denote the experimental or simulated output, sampled from the test data.

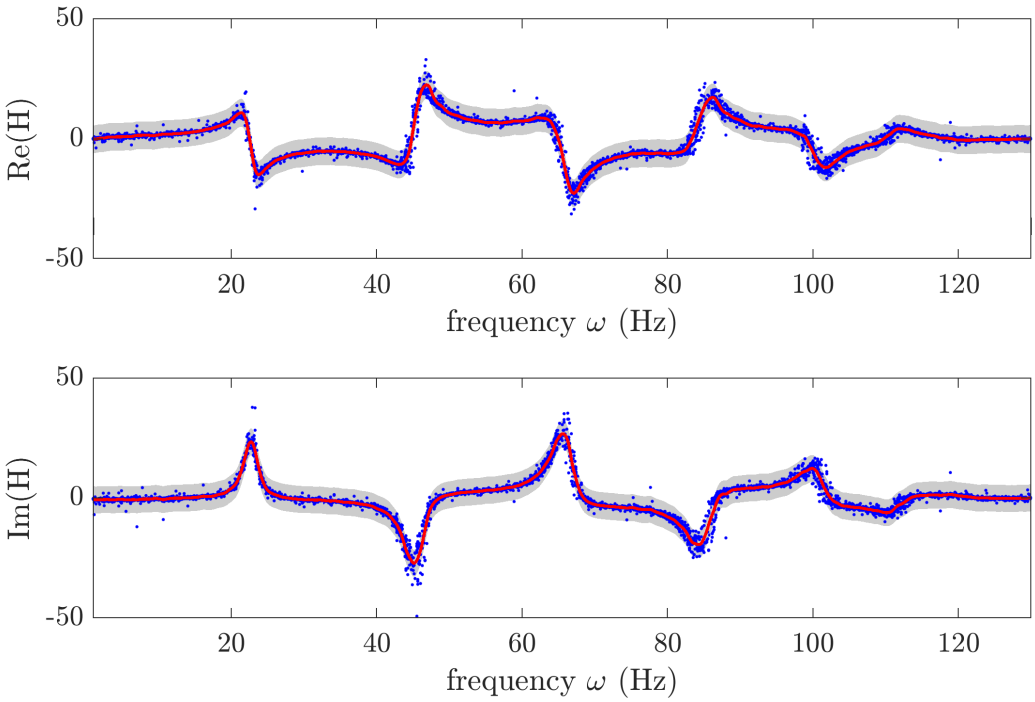

Figure 4: Gaussian process regression of the FRF as the population-form. Blue markers indicate the training-set. The red line indicates the mean prediction, $\mathbb{E}[y^*]$, and the shaded area indicates 3-σ uncertainty, corresponding to the variance, $\mathbb{V}[y^*]$.

In order to define a detection threshold, which flags an FRF in as either *inlying* or *outlying* (i.e. normal or novel), bootstrap-sampling is used [12, 16]. This defines the threshold by randomly sampling 1000 points from the normal-condition data used to train the form. The MSD_{FRF} is then calculated according to (12). These steps are repeated for a large number of trials, and the resulting MSDs are sorted in order of magnitude. The critical value is the threshold which contains 95.45% (two-sigma) of the MSD values beneath it.

3.3 Results

Results for novelty detection across the population via. the form are shown in Figures 5 and 6; these plots can be interpreted as a control chart, each sub-figure representing individual member. Figure 5 presents the MSD values (coresponding to test FRFs) for members $\{S_1, \dots, S_{10}\}$; these members contributed (a separate set of) normal-condition data used to train the form, shown in Figure 4. The MSD values for members $\{S_{11}, \dots, S_{20}\}$ are presented in Figure 6, including the experimental rig, S_{20}; importantly, these systems were in the hold-out group, that did not contribute data to train the form.

For the normal-condition test data, relating to the hold-out and training systems, the MSD discordancy measure generally falls below the detection threshold, for all members in the population. This is expected, as variation in these data (compared to the form) should mostly relate to measurement noise, as the parameters of the population, $\boldsymbol{\Theta}_i$, remain unchanged for each member.

There are some false positives present, corresponding to the normal condition FRFs; for example, S^4, S^{19} and S^{20}. As well as noise effects, these false-positives are likely to be due to more 'extreme' parameter sets being drawn from the underlying distribution $p(\boldsymbol{\Theta}_i)$ of the homogeneous population. Notably, for the experimental member S^{20}, a normal condition FRFs is flagged as an outlier, while the rest are close to the threshold. This is unsurprising, however, considering that this member did not contribute any training data to learn the form; additionally, errors in the estimated parameters from Table 1 will add to the discordancy.

Observing the MSD values from the damaged-condition FRFs, intuitively, the number of true positives increases as

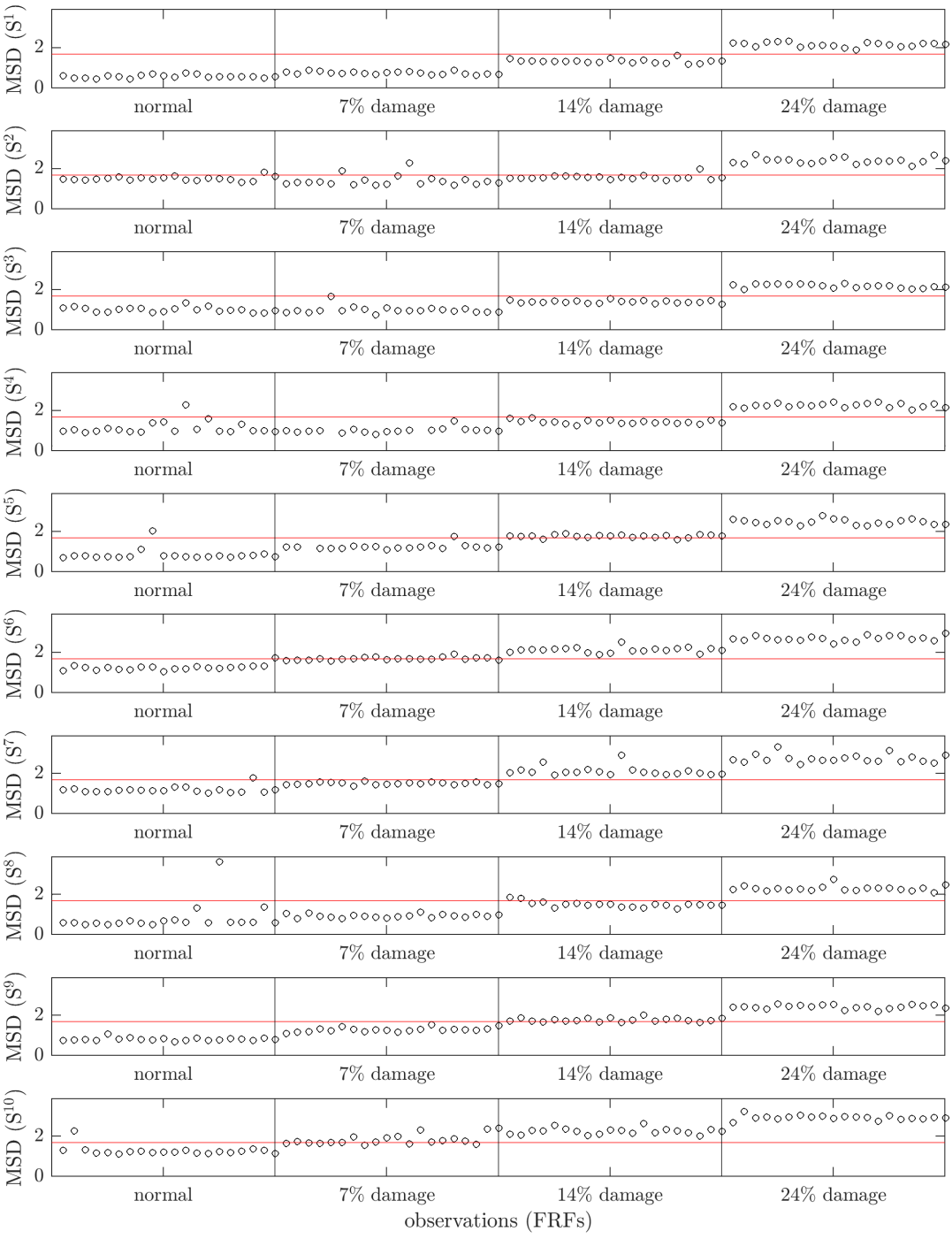

Figure 5: MSD novelty index for the test-data FRFs, comparing members $\{S^{10}, \ldots, S^{11}\}$ to the form. These members contributed a separate set of training data, used to learn the form. Damage/normal conditions are separated by vertical lines. The red line indicates the detection threshold.

.

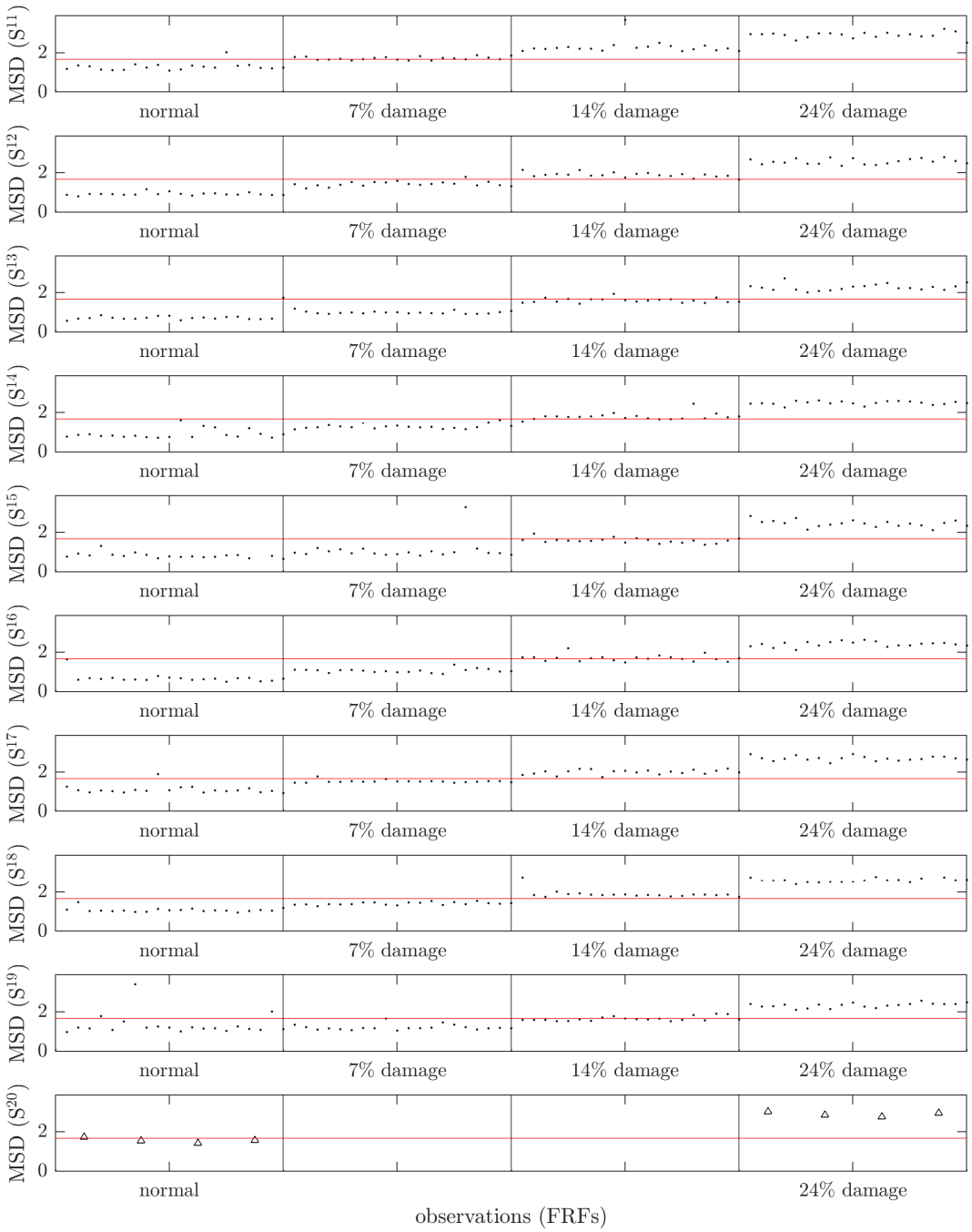

Figure 6: MSD novelty index for the test-data FRFs, comparing members $\{S^{11}, \ldots, S^{20}\}$ to the form. These members did not contribute training data to learn the form. Damage/normal conditions are separated by vertical lines. The $\bullet$ markers are used for simulated members $\{S^{11}, \ldots, S^{19}\}$, while $\triangle$ markers are used for the test-rig, member S^{20}. The red line indicates the detection threshold.

.

the severity of damage increases. Generally speaking, the form fails to highlight 7% damage, with increased sensitivity to 14% damage, and successfully flagging all 24% damage observations as as outlying. False negatives for 7% damage likely occur because, at low levels of damage, the variation across the population defined by $p(\boldsymbol{\Theta})$ is similar to (or more severe than) the the variations due to damage. As a result, with the current model of the form, variations within the normal-condition training data are *masking* the variations due to low-level damage. To expose low-level damage, another definition of the form is required; this can be done by defining an alternative feature-space, an alternative model, or both.

3.4 Discussion

This case study has demonstrated that the form can be used as a general representation of a strongly homogeneous population. Given training data from a *subset* of members, the form is able to model missing information from the hold-out group, to aid diagnostic decisions.

The success of this initial approach, however, depends greatly on $p(\boldsymbol{\Theta}_i)$, which, in turn, depends on the type of population. If the underlying density $p(\boldsymbol{\Theta}_i)$ across members is expected to be too dispersed and/or multi-modal (unlike the Gaussian distributions in this example) it is likely that the population variance will *mask* changes in the feature space that are due to damage, leading to false negatives. On the other hand, some of the (less frequent) population behaviour could fail to be captured in the training-set (and therefore the form) leading to false positives. As a result, in scenarios where $p(\boldsymbol{\Theta}_i)$ is complex – which, unsurprisingly, proves to be common in practical examples – conventional SHM can no longer be applied to the population, and more involved techniques should be investigated. An alternative technique is proposed in the next case study.

4 Case study 2: Beyond strongly-homogeneous – extending the form

In practice, the *strongly* homogeneous case breaks down for several reasons; for example, variations in the operational 'mass' would be expected for offshore structures, such as oil rigs, due to changes in the *variable load*; this could include additional loading from workforce, extracted materials, or helicopter landings. As a result, complex and multi-modal distributions would be associated with the parameters that define the mass of members across the population. Alternatively, when monitoring composite structures (such as wind-turbine blades), while the mass might remain relatively consistent, manufacturing tolerances are likely to lead to complicated distributions over the stiffness and damping parameters – before considering the potentially inconsistent boundary conditions.

As well as variations that can be described in terms of the structural parameters, the form should be capable of modelling additional *operational* variations, that do not relate to damage – in order to prevent unnecessary events from being flagged as outlying. For example, the data used to learn the form might change significantly upon operator involvement/control, or during maintenance procedures; while these changes are important, they do not indicate damage, or important novelty in the data, and should be modelled by the form appropriately.

4.1 Wind turbine population data

Using the measured data from an operational wind farm, a practical example of the form, and the *variance* that should be modelled by it, is introduced. The data were recorded from wind turbines owned by Vatenfall, using a Supervisor Control and Sensory Data Acquisition (SCADA) system [19, 20]. For confidentiality reasons, information regarding the specific type, location, and number of turbines cannot be disclosed. The data were recorded from a *homogeneous population* of systems over a period of 125 weeks [21, 20]. The mean value of the *power* produced and the measured *wind speed* are available over ten minute intervals. Through population-based SHM, the goal is to determine whether individual wind turbines within the farm are operating in a *permitted* normal state, or not.

In order to monitor the turbines using the available data, as in previous work [21, 20], the *power curve* method is used. Specifically, wind turbines are designed by manufacturers to have a specific relationship between the power produced and the wind speed; therefore, researchers have found that deviation between measured data and the power curve can be used to monitor the state of the turbine [21, 20]. As a visual example, power curves that would be considered normal (i.e. 'good') as well as 'bad' are presented in Figure 7, provided by Vatenfall [20].

Considering the framework introduced in the first case study, the power curve presents an ideal candidate (functional)

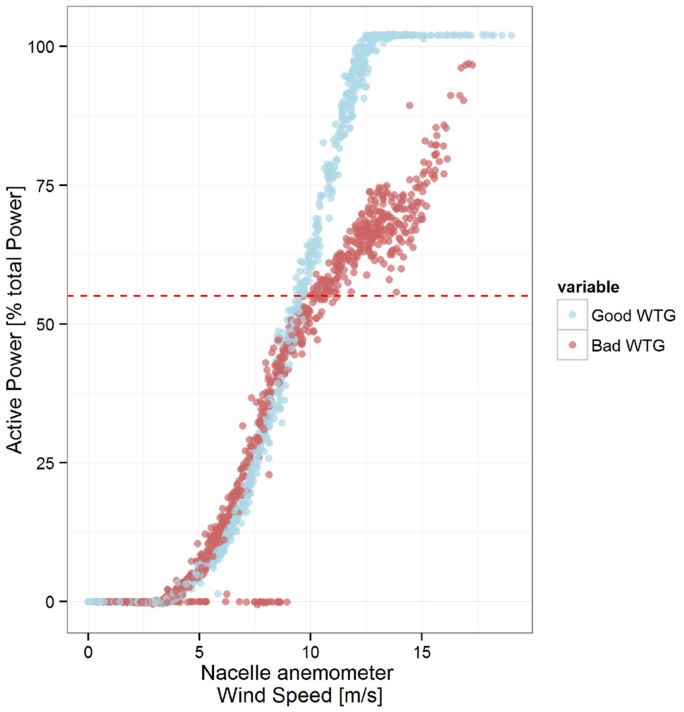

Figure 7: An example of a 'good' and 'bad' power curve. WTG stands for wind turbine generator. Figure provided by Vattenfall [20].

.

feature to learn the form, in order to monitor members within a population[2]. Various methods have been used to model the power curve in the literature [22, 23]; in line with previous studies [21, 20], as well of the first case study of this work, a method for GP regression will be used here.

4.1.1 Population variance in the power curve data

As the dataset contains 125 power curves for each turbine in the population (one curve per week), it is infeasible for an engineer to examine the entire dataset to label data that correspond to the normal operating condition. (In practice, the monitoring period will be significantly longer than the data presented here, and there may be many more members in the population.) Therefore, given expert knowledge, it is only possible to extract the normal-condition power curves from a *subset* of systems, and use these data to model the general population as a whole – following a similar procedure to training strategy proposed for the strongly-homogeneous case.

An example of the data that might represent the *ideal* normal-condition power curves is presented in Figure 8a, corresponding to a random sample from three members within the population, over three weeks of data. Given the feature space in Figure 8a, a single GP regression could be learnt (as demonstrated in Case Study I) in the hope that the resulting model would representative of the general population behaviour and variance. Unfortunately, however, there are important variations across the population that are not represented in these (ideal) data; in consequence, such a simple form would result in a large number of false positives – this issue is illustrated in the results.

For example, Figure 8b includes another random sample of data from three additional turbines, over another week of measurements. *Curtailments* can now be observed in the power curves of the population; these effects correspond to the the power-output of the wind turbine being limited or otherwise controlled by the operator. Interventions like this can occur frequently, and for various reasons – including maintenance or power requirements – they do not (normally) represent damage. Therefore, while the data in Figure 8b do not represent the ideal power curve, curtailments that are *known* to correspond to the normal condition should be included in the form, to prevent similar (future) activity from being flagged as outlying.

[2]Conveniently, this functional feature should be *more general* across the population than the FRF, as it is less sensitive to certain parameters (such as those associated with the boundary conditions) which introduce (less important) variation between members for the form.

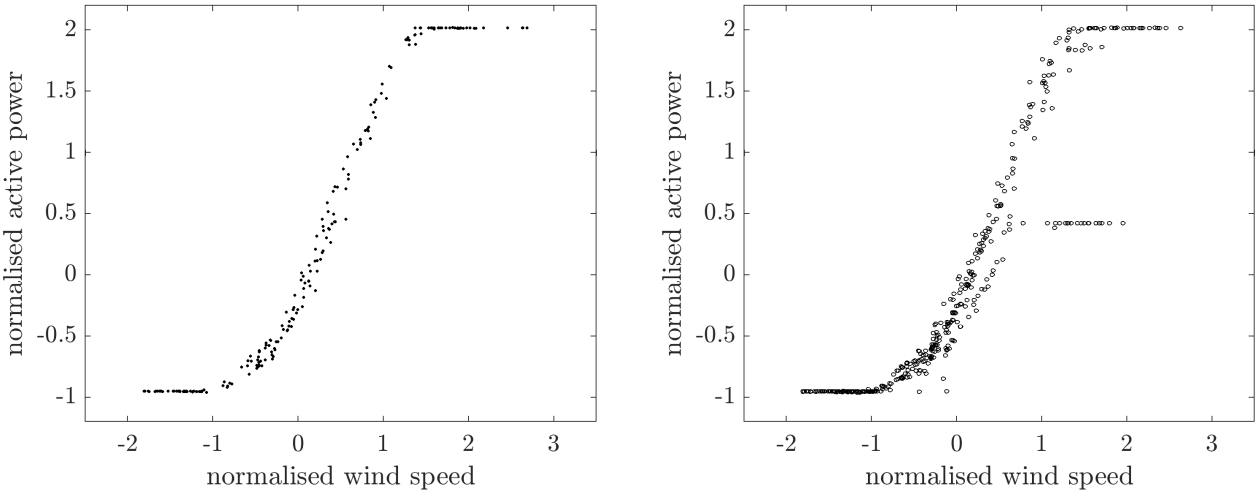

(a) (b)

Figure 8: Population power curve data. (a) A random sample of *ideal* data from four turbines over three weeks. (b) The data in (8a) as well as another sample from three additional turbines, including one extra week of measurements; these data include curtailments.

4.2 OMGP regression of the power curve as the population form

To model the data in Figure 8b, and to learn the form, an overlapping mixture of GP regressions (OMGP) is applied [11, 24]. Unlike the single GP, used in case study I, and previous studies, a mixture of regressions can capture the multi-functional behaviour of the normal-condition data across the population in the feature space; therefore, this method of modelling the form should be capable of representing more complex population behaviour. A (very) brief review of the model is provided; further details can be found in [11, 24] and will be discussed in future work.

The overlapping mixture of Gaussian processes (OMGP) assumes that there are K latent functions that describe the feature space,

$$\left\{ y^k = f^{(k)}(\mathbf{x}) + \epsilon_k \right\}_{k=1}^{K} \tag{14}$$

i.e. each output observation can be found by evaluating one of these functions, with additive Gaussian noise (as with a single GP (1), where $K = 1$). The function that generated each observation is unknown, therefore, a binary indicator matrix $\mathbf{Z}$ is introduced (as a latent variable), which defines the specific function associated with each observation: if the entry $[\mathbf{Z}]_{nk}$ is non-zero, this implies that the n^{th} data point was generated by the latent function k. Each observation can belong to one function only, thus there is only one non-zero term per row in $\mathbf{Z}$ [11].

Following a Bayesian framework, the following priors are placed over the latent variables and functions,

$$p(\mathbf{Z}) \;=\; \prod_{n=1,k=1}^{N,K} [\Pi]^{[\mathbf{Z}]_{nk}} \tag{15}$$

$$f^{(k)}(\mathbf{x}) \;\sim\; \mathcal{GP}\left(\mathbf{0}, k^{(k)}(\mathbf{x}, \mathbf{x}')\right), \qquad \epsilon_k \sim \mathcal{N}(0, \sigma^2_{(k)}) \tag{16}$$

they are a multinomial distribution, which is placed over the indicator matrix [10], a Gaussian distribution over the noise terms, and independent GP priors over each latent function [9]. As the computation of the posterior distribution $p\left(\mathbf{Z}, f^{(k)}(\mathbf{x}) \mid \mathcal{D}\right)$ is intractable, methods for approximate inference must be applied; specifically, a variational inference and expectation maximisation scheme is used [25]. This strategy iteratively computes the *approximate* posterior, and optimises the hyperparameters of the model, while an (improved) lower bound on the marginal likelihood is maximised [11].

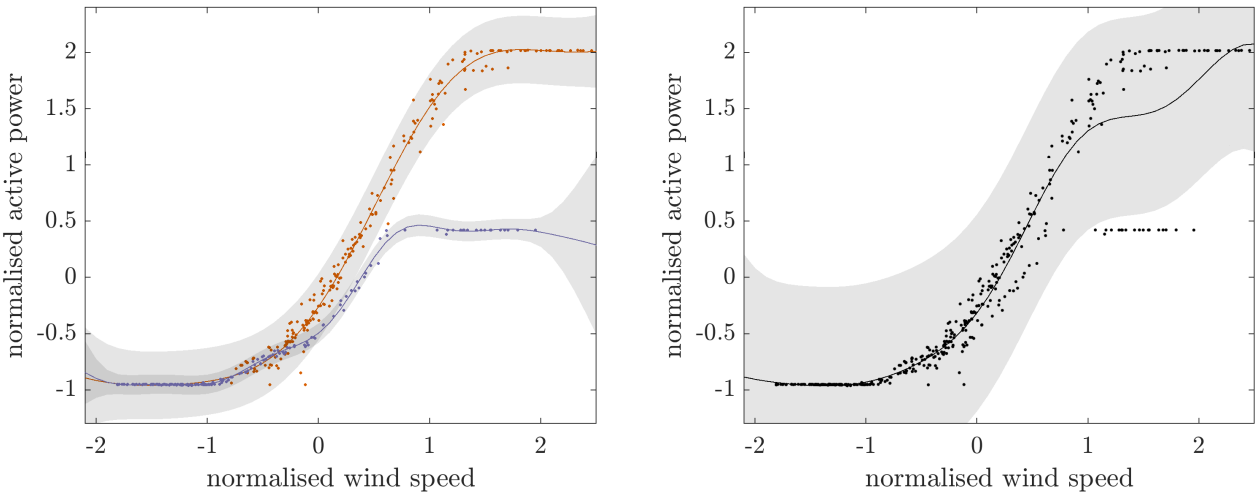

Figure 9: Gaussian process regression of the power curve as the population form (a) The overlapping mixture of GPs model (b) conventional GP regression. Shaded area shows three-sigma standard deviation.

To summarise, the OMGP model finds K latent functions, given a set of *unlabelled* input and output data; this is achieved using a variational approximation, to construct a (corrected) lower bound on the marginal likelihood, and then maximising this bound. When modelling the form from the data in Figure 8b, the number of latent functions is set to $K = 2$: prior knowledge informs us that there are two key characteristics in the feature space: data that represent the ideal power curve, and data that (likely) represent an operator limiting the power, leading to curtailments.

4.3 Results

The OMGP representation of the form is shown in Figure 9a; the model has automatically found two distinct latent functions, capturing the 'ideal' power curve data, as well as the curtailment behaviour – both of which have been assumed to represent (acceptable) normal conditions. For comparison, a conventional (single) GP was learnt for the same data, shown in Figure 9b; clearly, such a model of the from could mask variations due to damage, leading to numerous false negatives during the monitoring regime; additionally, data corresponding power curtailments (which are assumed to represent an acceptable normal condition) are likely to be indicated as outliers. To reiterate, only a *subset* of turbines contributed data to learn the form shown in Figure 9a.

To introduce the use of the OMGP to model the form for novelty detection, the mixture is compared to test-data from *all* turbines within the population, assessed via the MSD discordancy measure (12) as in case study I (the MSD corresponds to the most likely latent function). For the 125 (weekly) power curves from all wind turbines (other than those used for training) the distances were ranked, and the ten *most similar* and *most dissimilar* weeks were extracted from the corresponding turbines. Figure 10 plots two power curves, each extracted from a single turbine, sampled at random from each group of these groups.

An example of data that appear significantly different to the from are shown in Figure 10a; clearly these data are outlying, and most likely correspond to *inactive* turbines. Power curve data that gave a low MSD index are shown in Figure 10b – intuitively, compared to Figure 8a, these data are more representative of the ideal power curve.

5 Concluding Remarks

The concept of the *form*, used to represent a population of homogeneous systems, has been introduced for structural health monitoring. In two case studies, a statistically-modelled form was used to achieve damage detection across a simulated population, and measured data recorded from an operational wind farm. In these examples, Gaussian process models were used to learn functional features as the form; however, the choice of model (and feature space) is

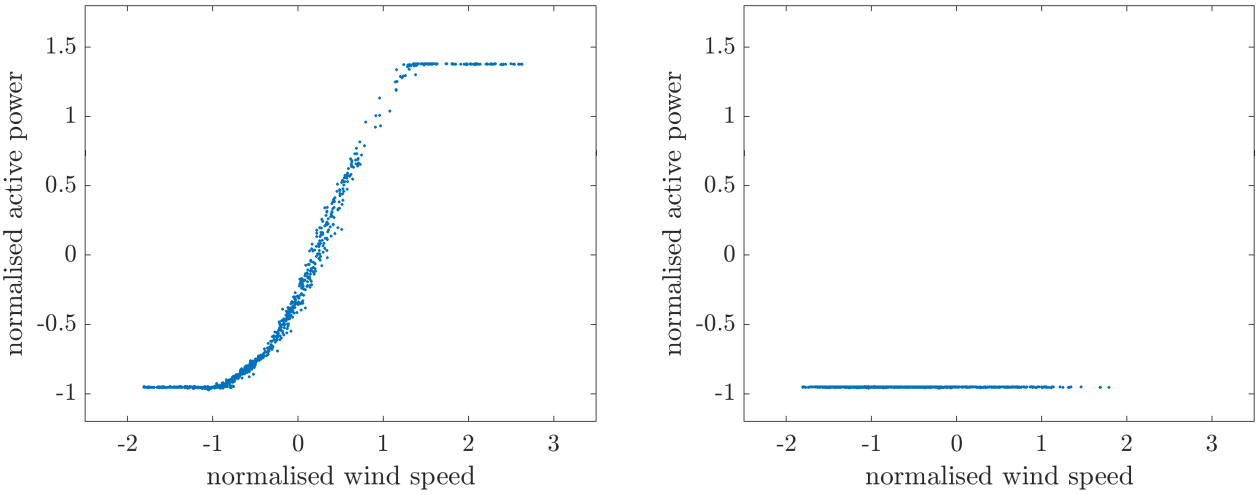

Figure 10: Examples of power curves (weekly) that were (a) similar to the OMGP modelled form (b) significantly different to the OMGP form.

flexible and application dependent. Importantly, the form is trained using various normal-condition data generated by *subsets* of members from the population only – this information is used in an attempt to learn a *shared* model, to represent the *general* population behaviour. Novelty detection was achieved through comparisons between each member in the population to the form, through the Mahalanobis squared-distance, for both the simulated and operational data.

The forms defined in this work (modelled by a standard Gaussian process, as well as a mixture of Gaussian process regressors) are just two methods to model shared information between structures. Alternative methods are being investigated within the same general framework (as well as alternative approaches to population-based SHM), for future work.

Acknowledgements

The authors gratefully acknowledge the support of the UK Engineering and Physical Sciences Research Council (EPSRC) through Grant references EP/R003645/1, EP/R004900/1 and EP/S001565/1.

References

[1] L.A. Bull, P.A. Gardner, J. Gosliga, T.J. Rogers, M. Haywood-Alexander, N. Dervilis, E.J. Cross, and K. Worden. Towards population-based structural health monitoring, Part I: Homogeneous populations and forms. In *Proceedings of IMAC XXXVIII – the 38th International Modal Analysis Conference, Houston, TX*, 2020.

[2] J. Gosliga, P.A. Gardner, L.A. Bull, N. Dervilis, and K. Worden. Towards population-based structural health monitoring, Part II: Heterogeneous populations and structures as graphs. In *Proceedings of IMAC XXXVIII – the 38th International Modal Analysis Conference, Houston, TX*, 2020.

[3] L. Bull, T.J. Rogers, N. Dervilis, E.J. Cross, and K. Worden. A Gaussian process form for population-based structural health monitoring. In *proceedings of the 13th International Conference on Damage Assessment of Structures (DAMAS 2019)*. Springer, 2019.

[4] J. Gosliga, P.A. Gardner, L.A. Bull, N. Dervilis, and K. Worden. Towards population-based structural health monitoring, Part III: Graphs, networks and communities. In *Proceedings of IMAC XXXVIII – the 38th International Modal Analysis Conference, Houston, TX*, 2020.

[5] P.A. Gardner and K. Worden. Towards population-based structural health monitoring, Part IV: Heterogeneous

populations, matching and transfer. In *Proceedings of IMAC XXXVIII – the 38th International Modal Analysis Conference, Houston, TX*, 2020.

[6] K. Worden. Towards population-based structural health monitoring, Part VI: Structures as geometry. In *Proceedings of IMAC XXXVIII – the 38th International Modal Analysis Conference, Houston, TX*, 2020.

[7] W. Lin, K. Worden, and E.J. Cross. Towards population-based structural health monitoring, Part VII: EoV fields: environmental mapping. In *Proceedings of IMAC XXXVIII – the 38th International Modal Analysis Conference, Houston, TX*, 2020.

[8] C.R. Farrar and K. Worden. *Structural Health Monitoring: a Machine Learning Perspective*. John Wiley and Sons, 2012.

[9] C.E. Rasmussen and C.K. Williams. *Gaussian Processes for Machine Learning*. The MIT Press, 2005.

[10] A. Gelman, H.S. Stern, J.B. Carlin, D.B. Dunson, A. Vehtari, and D.B. Rubin. *Bayesian Data Analysis*. Chapman and Hall/CRC, 2013.

[11] M. Lázaro-Gredilla, S.Ṽan Vaerenbergh, and N.D. Lawrence. Overlapping mixtures of gaussian processes for the data association problem. *Pattern Recognition*, 45:1386–1395, 2012.

[12] K.P. Murphy. *Machine Learning: a Probabilistic Perspective*. MIT press, 2012.

[13] D.J.C. MacKay. Bayesian model comparison and backprop nets. In *Advances in Neural Information Processing Systems*, pages 839–846, 1992.

[14] L. Ljung. *System Identification: Theory for the User*. Prentice-Hall PTR, 1987.

[15] R.N. Clark. *Control System Dynamics*. Cambridge University Press, 1996.

[16] K. Worden, G. Manson, and N.R.J. Fieller. Damage detection using outlier analysis. *Journal of Sound and Vibration*, 229:647–667, 2000.

[17] K. Worden and G.R. Tomlinson. *Nonlinearity in Structural Dynamics: Detection, Identification and Modelling*. CRC Press, 2000.

[18] J. Quiñonero-Candela and C.E. Rasmussen. A unifying view of sparse approximate gaussian process regression. *Journal of Machine Learning Research*, 6:1939–1959, 2005.

[19] W. Yang, R. Court, and J. Jiang. Wind turbine condition monitoring by the approach of SCADA data analysis. *Renewable Energy*, 53:365–376, 2013.

[20] E. Papatheou, N. Dervilis, A.E. Maguire, C. Campos, I. Antoniadou, and K. Worden. Performance monitoring of a wind turbine using extreme function theory. *Renewable Energy*, 113:1490–1502, 2017.

[21] E. Papatheou, N. Dervilis, A.E. Maguire, I. Antoniadou, and K. Worden. A Performance Monitoring Approach for the Novel Lillgrund Offshore Wind Farm. *IEEE Transactions on Industrial Electronics*, 62:6636–6644, 2015.

[22] T. Ouyang, A. Kusiak, and Y. He. Modeling wind-turbine power curve: A data partitioning and mining approach. *Renewable Energy*, 102:1–8, 2017.

[23] V. Thapar, G. Agnihotri, and V.K. Sethi. Critical analysis of methods for mathematical modelling of wind turbines. *Renewable Energy*, 36:3166–3177, 2011.

[24] C. Tay and C. Laugier. Modelling smooth paths using Gaussian processes. In *Proceedings of the International Conference on Field and Service Robotics*.

[25] D.M. Blei, A. Kucukelbir, and J.D. McAuliffe. Variational inference: A review for statisticians. *Journal of the American Statistical Association*, 112:859–877, 2017.